Optical emission properties of Nd³⁺ in NaBi(WO₄)₂ single crystal

A. MÉNDEZ-BLAS, M. RICO, V. VOLKOV, C. ZALDO† and
C. CASCALES*

Instituto de Ciencia de Materiales de Madrid, Consejo Superior de Investigaciones
Científicas, Cantoblanco, E-28049 Madrid, Spain

Room temperature optical absorption measurements of Nd³⁺ in NaBi(WO₄)₂ single crystals grown by the Czochralski method have been used to calculate the following Judd–Ofelt intensity parameters: $\Omega_2 = 30.9 \times 10^{-20}\,\text{cm}^2$, $\Omega_4 = 12.0 \times 10^{-20}\,\text{cm}^2$ and $\Omega_6 = 9.3 \times 10^{-20}\,\text{cm}^2$. Using these parameters the emission properties of Nd³⁺ in this host have been estimated with particular attention to the $^4F_{3/2}$ energy level responsible for stimulated emission channels. The experimental branching ratios of this level are obtained from photoluminescence and agree with those calculated using the above Ω_k parameters. The $^4F_{3/2}$ emission has negligible non-radiative intrinsic losses and the 10 K lifetime at low Nd concentration, $0.9 \times 10^{18}\,\text{cm}^{-3}$, is $\tau_{\text{exp}} = 143\,\mu\text{s}$. Even at 300 K and for a much higher Nd concentration, $4.0 \times 10^{19}\,\text{cm}^{-3}$, non-radiative losses are moderate, giving a quantum efficiency $\eta \approx 0.85$. The $^4F_{3/2}$ emissions show a strongly polarized character. The largest emission cross-section occurs at $\lambda = 1060.9\,\text{nm}$ for the $^4F_{3/2} \rightarrow {}^4I_{11/2}$ laser channel with a π-polarized character, $\sigma_{\text{EMI}} = 16 \times 10^{-20}\,\text{cm}^2$.

1. Introduction

Double tungstate NaBi(WO₄)₂ (hereafter denoted as NBW) single crystal is a prospective material for solid state Raman laser shifting because of its high cubic non-linear susceptibility, $\chi^{(3)}$ [1]. This crystal adopts a tetragonal structure derived from the CaWO₄ scheelite structure-type by the substitution of Ca²⁺ for Na⁺ and Bi³⁺ simultaneously. The space group of the crystal symmetry is I$\bar{4}$ [2–4]. The crystal is optically uniaxial, with the optic axis parallel to the crystalline c axis. Furthermore, such NBW crystal is considered a locally disordered host as a consequence of the random distribution of Na⁺ and Bi³⁺ ions over two non-equivalent crystal sites, which are populated with a different Na/Bi ratio.

So far, undoped NBW has been used to shift the Nd emission of an external laser [5]. The incorporation of Nd ions into NBW crystal would offer the opportunity of stimulated emission and Raman shifting in a single crystal piece. This task seems possible as NBW:Nd has been reported as a laser system [6] although details on the performance are not available in the open literature. Nevertheless, this achievement may not be easy because of the existence of limits to the neodymium incorporation in NBW [7, 8]. The purpose of the present work is to explore the emission capabilities of Nd³⁺ in NBW to

guide future attempts to grow Nd-doped NBW with Nd concentration and optical quality suitable for laser operation.

The optical properties of Nd³⁺ in the NBW host, in which Bi³⁺ is partially replaced by Nd³⁺, are closely related to the local structure and bonding around Nd³⁺. In fact, previous works [9] have shown that, independently of the Nd concentration, the 10 K optical absorption band widths are in the 15–30 cm⁻¹ energy range. This is clearly larger than the absorption linewidths observed in typical laser hosts. For instance, the FWHM (full width at half maximum) of the Stark components of the $^4I_{9/2} \rightarrow {}^4F_{5/2}$ neodymium absorption (a typical diode pumping channel) is ≈2.2 cm⁻¹ in YAG and ≈15 cm⁻¹ in NBW. This feature strongly suggests slight site-to-site variations of the crystal field derived from the different short-range Na⁺ and Bi³⁺ distributions around the Nd³⁺ optical centres present in the host. Broad absorption and emission linewidths may find specific applications in laser devices, like laser tunability, improved absorption efficiency of the diode pumping or suitability for hole burning optical memories.

From the crystal-field analysis of the 10 K optical absorption (OA) and photoluminescence (PL) spectra, the labelled $^{2S+1}L_J$ sequence of energy levels from $^4I_{9/2}$ to $^2I_{11/2}$ for Nd³⁺ in NBW has been previously reported [9]. In the present work, we expand the spectroscopic analysis with particular attention to aspects concerning the 300 K emission efficiency of Nd³⁺ in NBW. We have determined the 300 K OA of Nd³⁺ and applied the

* Author for correspondence. e-mail: ccascales@icmm.csic.es

† e-mail: cezaldo@icmm.csic.es

Judd–Ofelt (JO) formalism to obtain the theoretical branching ratios and radiative rates. The consistency of this analysis has been tested by comparing the theoretical and experimental branching ratios. Finally, non-radiative de-excitation processes are investigated as a function of the Nd concentration through the determination of the experimental $^4F_{3/2}$ emission lifetimes.

2. Experimental techniques

Three NBW:Nd^{3+} single crystals with increasing Nd concentrations in the melt (0.003%, 0.014% and 0.06% in weight) have been grown by the Czochralski method. Details of the crystal growth procedure have been given elsewhere [7, 8]. The highest Nd concentration in the crystal, measured by total reflection X-ray fluorescence (TXRF) and by proton induced X-ray emission (PIXE) techniques, was $[Nd] = 0.28 \pm 0.03 \times 10^{19}\,cm^{-3}$.

Polarized OA spectra were recorded at 300 K by using a Varian 5E spectrophotometer and a Glan–Taylor polarizer. Polarized continuous wave photoluminescence (cw-PL) was excited with the $\lambda = 514.5\,nm$ emission of an Ar^+ laser, the neodymium emission was selected by the above polarizer, analysed with a Spex 340E spectrometer and finally detected with a 77 K cooled Ge photodiode and a lock-in amplifier. The spectral response of this equipment was obtained by measuring the emission of a calibrated EGG quartz tungsten halogen lamp and used to obtain corrected cw-PL spectra.

The fluorescence lifetime of the $^4F_{3/2}$ multiplet was measured for the Nd concentrations available, in the 10–300 K temperature range. A pulsed dye laser (DUO-220, LSI) tuned either at $\lambda = 514\,nm$ ($^4G_{9/2} + ^2K_{13/2}$ excitation) or at $\lambda = 590\,nm$ ($^4G_{5/2}$ excitation) was used. It is well known that these upper levels decay non-radiatively to the $^4F_{3/2}$ multiplet in a time much shorter than the corresponding radiative and measured lifetimes of $^4F_{3/2}$ [10, 11], and for that reason the pumping schemes used here allow meaningful $^4F_{3/2}$ lifetime measurements. Within the experimental uncertainty, no difference in the $^4F_{3/2}$ lifetime was found between the two above pumping wavelengths. The light emitted by the $^4F_{3/2} \rightarrow\,^4I_{9/2}$ transition ($\lambda_{em} \approx 890\,nm$) was dispersed by a 0.5M SPEX monochromator and detected by a cooled Hamamatsu R636 photomultiplier. The signal was stored and averaged in a Tektronix 2440 oscilloscope. Sample temperature was controlled by using a He closed-cycle cryostat.

3. Experimental results

Figure 1 gives an overview of the 300 K π ($\mathbf{E}||c$, $\mathbf{B} \perp c$) and σ ($\mathbf{E} \perp c$, $\mathbf{B}||c$) polarized OA spectra of Nd^{3+} in NBW. The overlap bands observed have been ascribed to nine sets of Nd^{3+} multiplets, in accordance with the
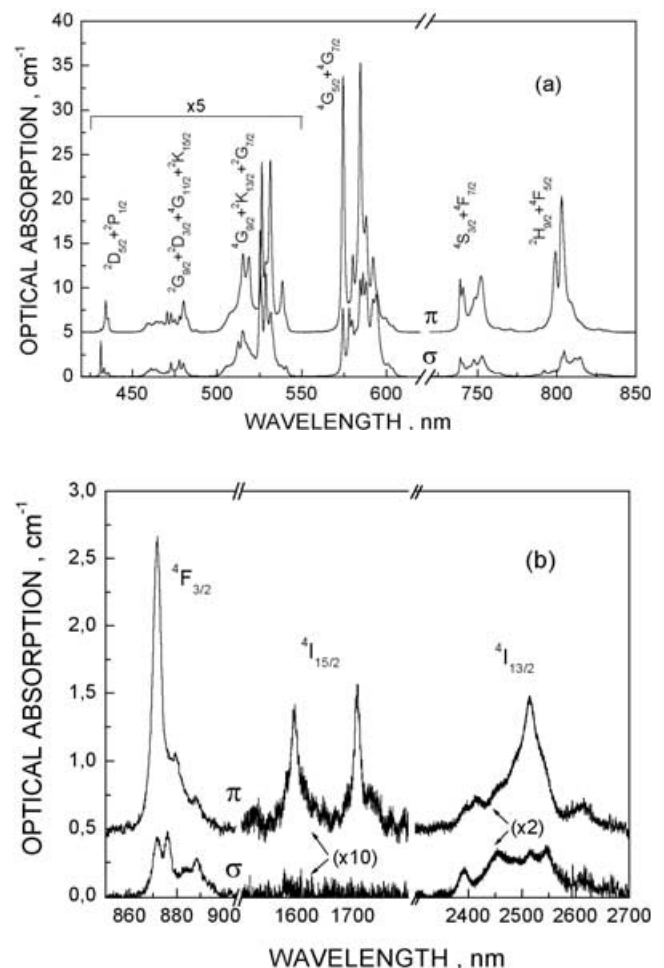

Figure 1. Ground state ($^4I_{9/2}$) polarized optical absorption of Nd^{3+} in NBW crystal measured at 300 K. $[Nd] = 4.0 \times 10^{19}\,cm^{-3}$. (*a*) Visible and near-infrared region. π spectrum is shifted $5\,cm^{-1}$ on the *y* axis. (*b*) Middle-infrared region. π spectrum is shifted $0.5\,cm^{-1}$ on the *y* axis.

relative energy of the Stark levels established after the proper 10 K OA measurements and crystal field analysis previously published [9]. Obviously, the OA broadening observed at 300 K with regards to 10 K OA bands mainly arises from the thermalization of the ground state electron population. The two typical Nd channels for diode pumping are the $^4F_{3/2}$ and $^4F_{5/2}$ multiplet absorptions. The $^4F_{3/2}$ multiplet appears rather isolated around $\sim 870\,nm$ ($11\,494\,cm^{-1}$) and with a high energy component strongly π polarized. On the other hand, the $^4F_{5/2}$ multiplet appears overlapped to the $^2H_{9/2}$ one and is also strongly π polarized.

From the 300 K OA measurements displayed in figure 1 the integrated optical absorption, i.e. $\Gamma_{JJ'} = \int \alpha(\lambda)\,\partial\lambda$, is calculated. The experimental oscillator strengths, f_{exp}, are obtained as

Table 1. Room temperature experimental oscillator strengths $f_{\exp}(\times 10^{-8})$ determined from the optical absorption ([Nd] $= 4 \times 10^{19}\,$cm^{-3}) and calculated $f_{\mathrm{cal}}(\times 10^{-8})$ using the Ω_k parameters obtained from the Judd–Ofelt analysis. $\bar{\lambda}$ indicates the average multiplet set spectral position.

$^4I_{9/2} \rightarrow {}^{2S+1}L_J$	$\bar{\lambda}$ (nm)	$f_{\exp\sigma}$	$f_{\exp\pi}$	$\bar{f}_{\exp}$	f_{cal}
$^4I_{13/2}$	2508	125	187	146	413
$^4I_{15/2}$	1651	0.316	58	19.6	61
$^4F_{3/2}$	879	238	591	358	914
$^2H_{9/2} + {}^4F_{5/2}$	809	1845	5029	2920	2460
$^4S_{3/2} + {}^4F_{7/2}$	750	1665	4241	2520	2230
$^4G_{5/2} + {}^2G_{7/2}$	586	14 512	20 362	16 537	16 600
$^4G_{9/2} + {}^2K_{13/2} + {}^4G_{7/2}$	524	2452	4624	3172	2930
$^2G_{9/2} + {}_2^2D_{3/2} + {}^4G_{11/2} + {}^2K_{15/2}$	472	381	950	570	515
$^2P_{1/2} + {}^2D_{5/2}$	433	287	600	389	297
$\Omega_2 = 30.9 \times 10^{-20}\,$cm^2		$\Omega_4 = 12.0 \times 10^{-20}\,$cm^2		$\Omega_6 = 9.3 \times 10^{-20}\,$cm^2	RMS $= 3.6 \times 10^{-20}\,$cm^2

$$f_{\exp} = \frac{4\varepsilon_0 mc^2}{[\mathrm{Nd}]e^2\bar{\lambda}^2}\Gamma_{JJ'}, \qquad (1)$$

where c is the vacuum speed of the light, ε_0 is the vacuum dielectric permitivity, m and e are the electron mass and charge respectively and $\bar{\lambda}$ is the average wavelength of the $J \rightarrow J'$ transition. Table 1 summarizes the σ and π experimental oscillator strengths for the $^{2S+1}L_J$ multiplet sets observed in Nd-doped NBW. The Nd concentration used in this table was consistent with the JO analysis described later.

The Nd^{3+} most important laser-related transitions, $^4F_{3/2} \rightarrow {}^4I_J$ ($J = 9/2, 11/2, 13/2$), are show in figure 2. As in most laser hosts the $^4F_{3/2} \rightarrow {}^4I_{15/2}$ was too weak and its intensity could not be distinguished from the equipment noise. For all Nd concentrations available the emissions observed consist of broad and overlapped bands. This is a specific characteristic of the Nd^{3+} spectra in NBW and it has nothing to do with limitations in the spectral resolution of our measurements. This broad character of the emission has also been observed in other partially disordered tungstate hosts, for instance in KLa(MoO$_4$)$_2$ [12] or NaY(WO$_4$)$_2$ [1, 13]. In comparison to these two latter compounds our emission bands are much alike to those observed for NaY(WO$_4$)$_2$, see figure 3 of [1] or figure 5 of [13], and narrower than those reported for KLa(MoO$_4$)$_2$ [12].

The accurate correction of the cw-PL spectra by the equipment response confers reliability to the current results, and it allows comparison of the intensities of the three infrared PL bands observed in figure 2. The experimental branching ratios, $\beta_{\exp}$, for inter-manifold multiplet transitions are defined as

$$\beta_{\exp} = \frac{\int_{\lambda_i}^{\lambda_f} I_J(\lambda)\,\mathrm{d}\lambda}{\sum_k \int_{\lambda_i}^{\lambda_f} I_k(\lambda)\,\mathrm{d}\lambda}, \qquad (2)$$

where k runs over all the integrated area of the considered transitions. In our case, for the uniaxial crystal considered, the spectrum intensities were averaged according to their polarization character as $I_J = (2I_J^\sigma + I_J^\pi)/3$. Table 2 summarizes the $\beta_{\exp}$ values obtained.

The experimental lifetime of the $^4F_{3/2}$ multiplet was first studied for the lowest Nd concentration available (0.003%, [Nd] $= 0.9 \times 10^{18}\,$cm^{-3}, see discussion later). At this concentration, the average Nd–Nd distance is about 64 Å, so resonant energy transfer can be neglected. At 10 K the light intensity decay follows an exponential law, and the experimental lifetime found
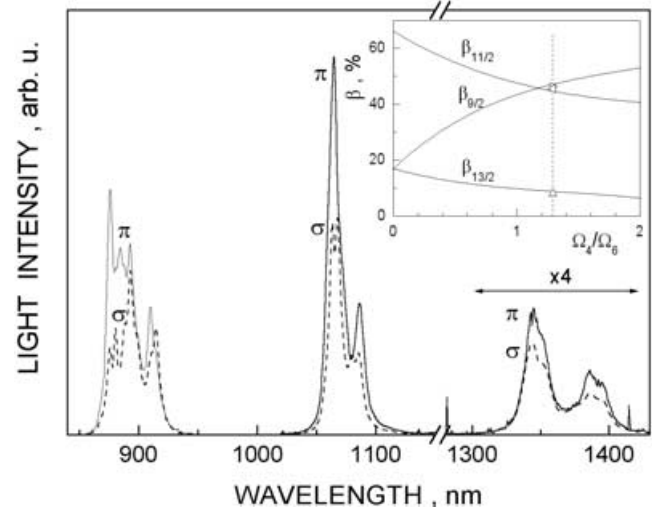

Figure 2. Polarized $^4F_{3/2} \rightarrow {}^4I_J$ photoluminescence of Nd^{3+} in NBW measured at 300 K. The spectra shown are corrected by the spectral response of the equipment. π polarized, continuous line. σ-polarized, dashed line. The inset shows the agreement among calculated and experimental $^4F_{3/2}$ branching ratios with the quality factor Ω_4/Ω_6: ▷, $\beta_{9/2}$; ◁, $\beta_{11/2}$; △, $\beta_{13/2}$.

Table 2. Spontaneous emission probabilities A, radiative branching ratios β and radiative lifetime τ_{rad} for $^{2S+1}L_J$ multiplet of Nd^{3+} in $NaBi(WO_4)_2$ single crystal. The experimental branching ratios, β_{exp}, and lifetimes, τ_{exp}, of the lowest concentrated sample are also included for comparison.

Initial state	Final state	$A(\mathrm{s}^{-1})$	$\beta_{\mathrm{th}}, \beta_{\mathrm{exp}}(\%)$	$\tau_{\mathrm{rad}}, \tau_{\mathrm{exp}}(\mu\mathrm{s})$
$^4G_{9/2}$				7
$^2G_{7/2}$				10
$^4G_{7/2}$				8
$^4G_{5/2}$				15
$^4S_{3/2}$				0.1
$^4F_{7/2}$				53
$^4F_{5/2}$				74
$^4F_{3/2}$	$^4I_{9/2}$	3345	47.4, 46.3	142, 143 (10 K); 137 (300 K)
	$^4I_{11/2}$	3315	44.1, 45.6	
	$^4I_{13/2}$	574	8.1, 8.1	
	$^4I_{15/2}$	30	0.4, —	
$^4I_{15/2}$				2800
$^4I_{13/2}$				3900
$^4I_{11/2}$				17 700

is $\tau_{\mathrm{exp}} = 143\,\mu\mathrm{s}$. Figure 3 shows that this value decreases slowly with increasing temperature, but still a single exponential is found, see figure 4(*a*). The room temperature lifetime was $\tau_{\mathrm{expRT}} = 136.6\,\mu\mathrm{s}$. Faster light intensity decays are observed at higher Nd concentrations. Even for the highest one available, $[\mathrm{Nd}] = 4.0 \times 10^{19}\,\mathrm{cm}^{-3}$ (Nd–Nd average distance $\approx 18\,\text{Å}$), the departure from the single exponential behaviour observed is minor, see figure 4(*c*). A more detailed discussion of this case follows in section 5, but for the moment we can keep in mind $\tau_{\mathrm{expRT}} = 121\,\mu\mathrm{s}$ as a rough approximation.
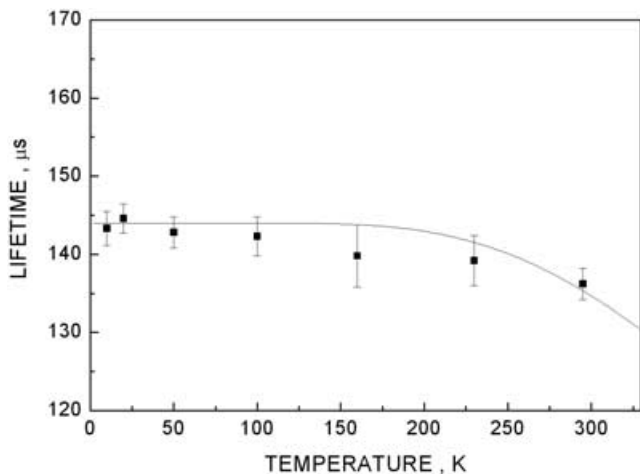

Figure 3. Temperature dependence of the $^4F_{3/2}$ experimental lifetime of Nd^{3+} in NBW. $\lambda_{\mathrm{emi}} = 890\,\mathrm{nm}$ ($^4F_{3/2} \rightarrow {}^4I_{9/2}$ emission band). The dots are the experimental values and the continuous line is the fit obtained by using equation (11) with $ph = 5.5$ and $\hbar\omega = 920\,\mathrm{cm}^{-1}$.

4. Judd–Ofelt calculations

The JO theory [14, 15] is often used to determine the radiative rates of the manifold $^{2S+1}L_J$ levels. The oscillator strength for an electric dipole (ED) transition between $4f^n[L,S]J$ and $4f^n[L',S']J'$ states is

$$f_{\mathrm{ED}} = \chi \frac{8\pi^2 mc}{3h\bar{\lambda}(2J+1)} S_{JJ'}, \qquad (3)$$

where $\chi = (n^2+2)^2/9n$ (n stands for the refractive index), h is the Planck constant and the line strengths are $S_{JJ'} = \sum_{k=2,4,6} \Omega_k |\langle 4f^n[L,S]J\|U^k\|4f^n[L',S']J'\rangle|^2$. Ω_k are the adjustable JO parameters and the reduced matrix elements corresponding to the $J \rightarrow J'$ transition of Nd^{3+}, $\langle\|U^k\|\rangle$, have been tabulated previously [16, 17]. The average spectral position, $\bar{\lambda}$, and experimental oscillator strengths of the nine 300 K OA band sets described in figure 1 and summarized in table 1 were considered to calculate the Ω_k parameters. Although there are some magnetic-dipole contributions, i.e. $^4I_{9/2} \rightarrow {}^2H_{9/2}$ and $^4I_{9/2} \rightarrow {}^2G_{7/2}$ transitions [18], these are small and have been neglected.

The application of JO theory to anisotropic solids requires the average of the experimental optical properties [19]. The average oscillator strength $\bar{f}_{\mathrm{exp}}$ for uniaxial systems is defined as $\bar{f}_{\mathrm{exp}} = (2f_{\mathrm{exp}\sigma} + f_{\mathrm{exp}\pi})/3$. In the calculation we have used the proper refractive indices of NBW at the corresponding $\bar{\lambda}$ of the multiplet [8]. Using the nominal Nd concentration obtained from the TXRF and PIXE measurements we arrived at radiative lifetimes $\approx 20\%$ shorter than the $^4F_{3/2}$ lifetime determined experimentally at 10 K for low Nd concentration. It was therefore obvious that the actual concentration of the sample used in this spectroscopic characterization
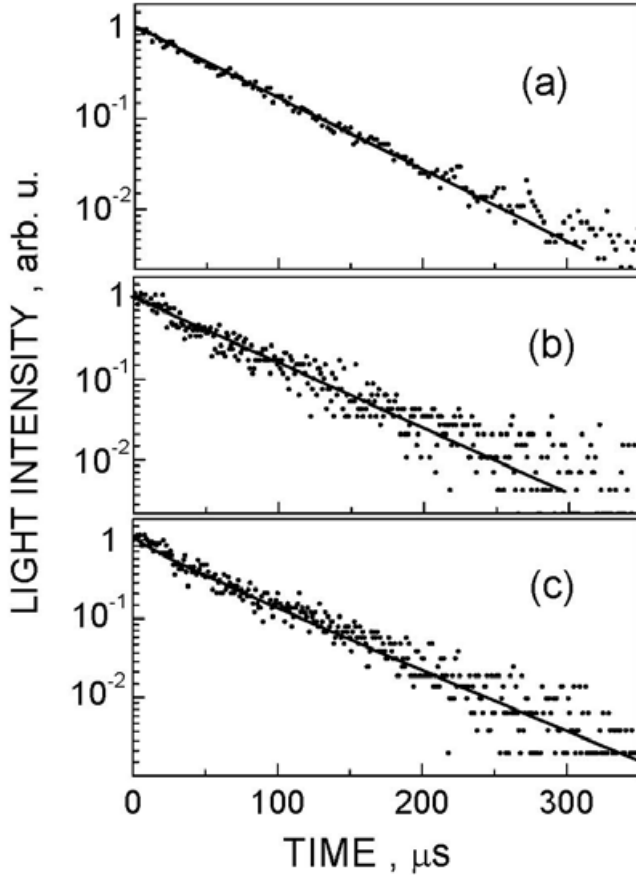
Figure 4. Room-temperature experimental lifetime decays of the $^4F_{3/2}$ level of Nd^{3+} in NBW. $\lambda_{EMI} = 890$ nm ($^4F_{3/2} \rightarrow {}^4I_{9/2}$ emission band). The dots are the experimental values and the continuous traces the exponential fits. (*a*) [Nd] $= 0.9 \times 10^{18}$ cm^{-3}, $\tau_{exp} = 137$ µs. (*b*) [Nd] $= 3.6 \times 10^{18}$ cm^{-3}, $\tau_{exp} = 128$ µs. (*c*) [Nd] $= 4.0 \times 10^{19}$ cm^{-3}. Fit with equation (12), $s = 6$ and $R_C = 9.6$ Å ($\tau_{exp} \approx 121$ µs).

was slightly higher than the nominal concentration obtained by TRFX and PIXE for the crystal boule. Therefore, we chose to use [Nd] as a further adjustable parameter which, while modifying Ω_k and τ_{rad} values, does not influence the $\beta_{JJ'}$ results and only to a minor extent the Ω_4/Ω_6 ratio. A good fit was found using [Nd] $= 4 \times 10^{19}$ cm^{-3}. Throughout the work we have used this Nd concentration and the corresponding integrated optical absorptions to calculate [Nd] in the two other samples used. Table 1 shows the Ω_k set obtained by minimizing the $\sum_{J'} (\bar{f}_{exp} - f_{ED})^2$ differences. The quality of the fit is described by the root mean square deviation, RMS $= [\sum_{i=1}^{q} (\Delta f_i)^2/(q-3)]^{1/2}$, where Δf_i are the residuals between the experimental ($\bar{f}_{exp}$) and calculated (f_{cal}) oscillator strengths and q is the number of transitions used in the fit. The value of the RMS deviation in the case of NaBi(WO$_4$)$_2$:Nd^{3+} is

about 5%. This is similar to the quality of previous fits in different hosts [17, 20].

The oscillator strength of the $^4I_{9/2} \rightarrow {}^4G_{5/2} + {}^4G_{7/2}$ transition is 6 times greater than those of the other bands (see table 1). This implies a high value for the Ω_2 parameter ($\Omega_2 = 30.9 \times 10^{-20}$ cm^2). However, this has no practical effect on the emission properties of the $^4F_{3/2}$ state, since these properties only depend on the Ω_4 and Ω_6 parameters [6].

The Ω_k JO parameters are now used to calculate the whole set of radiative rates, $A_{JJ'}$, for $J \rightarrow J'$ ED transitions, according to the formula

$$A_{EDJJ'} = \chi \left[\frac{16\pi^3 e^2}{3h\varepsilon_0 \bar{\lambda}^3} \right] \frac{n^2}{(2J+1)}$$
$$\times \sum_{k=2,4,6} \Omega_k |\langle 4f^n[L,S]J \| U^k \| 4f^n[L',S']J' \rangle|^2$$

$$(4)$$

although for the sake of brevity, table 2 summarizes only the calculated radiative rates of Nd^{3+} transitions related to possible laser channels. From the whole $A_{EDJJ'}$ set it was possible to obtain theoretical branching ratios, $\beta_{JJ'} = A_{JJ'}/\sum_{J'} A_{JJ'}$, and the radiative lifetimes, $\tau_{rad} = 1/\sum_{J'} A_{JJ'}$. Since we are mainly interested in the $^4F_{3/2}$ level, the whole $\beta_{JJ'}$ and τ_{rad} results are given in table 2 for this multiplet while for others only τ_{rad} values are provided.

5. Discussion

The probability of spontaneous transitions $A_{JJ'}$ for various $^4F_{3/2} \rightarrow {}^4I_J$ channels depends primarily on the Ω_4 and Ω_6 intensity parameters, since the matrix element $\langle \| U^2 \| \rangle$ for transitions between these states is equal to zero ($|\Delta J| > 2$). Hence the inter-manifold luminescence branching ratios $\beta_{JJ'}$ can be represented as a function of a single spectroscopic-quality parameter

$$X_{Nd}(^4F_{3/2}) = \frac{\Omega_4}{\Omega_6}. \qquad (5)$$

The analytical dependence of $\beta_{JJ'}$ is expressed as

$$\beta_{JJ'}(X_{Nd}) = \frac{(a_{J'}X_{Nd} + b_{J'})\lambda_{JJ'}^3}{\sum_{J'} (a_{J'}X_{Nd} + b_{J'})\lambda_{JJ'}^3}, \qquad (6)$$

where the $a_{J'}$ and the $b_{J'}$ constants are equal to the squared matrix elements of the irreducible tensor operators of rank 4 and 6,

$$a_{J'} = |\langle ^4F_{3/2} \| U^4 \| ^4I_{J'} \rangle|^2 \qquad (7)$$

and

$$b_{J'} = |\langle ^4F_{3/2} \| U^6 \| ^4I_{J'} \rangle|^2. \qquad (8)$$

According to the above JO analysis, the spectroscopic quality parameter for Nd^{3+} in NBW is $X = \Omega_4/\Omega_6 = 1.29$. Figure 2 inset and table 2 show a comparison of the calculated and experimental branching ratios of the $^4F_{3/2} \rightarrow {}^4I_J$ ($J = 9/2, 11/2, 13/2$) transitions of interest. The agreement is very good showing the consistency of the experimental and theoretical methods.

In order to estimate the spontaneous emission cross-sections, σ_{EMI}, of the laser channels related to the $^4F_{3/2}$ multiplet we have first applied the reciprocity principle [21] to the $^4I_{9/2} \leftrightarrow {}^4F_{3/2}$ transition where the ground state absorption cross-sections, σ_{GSA}, are known for both polarizations (figure 1 (b)). The emission cross-section of the fluorescence band around 900 nm is calculated as

$$\sigma_{EMI} = \sigma_{GSA} \frac{Z_l}{Z_u} \exp\left[(E_{zl} - h\nu)/k_B T\right], \qquad (9)$$

where $\sigma_{GSA}(\lambda) = \alpha(\lambda)/[Nd]$, Z_u and Z_l are the partition functions of the upper and lower multiplets respectively, E_{zl} is the energy gap between the lowest Stark levels of these two multiplets, k_B is the Boltzmann constant and T is the sample temperature. Figure 5 shows a comparison of the calculated emission cross-section and the experimental photoluminescence spectral distributions in both polarization configurations. Apart from a small mismatch (<0.5 nm) due to the different spectral calibrations of the absorption spectrophotometer and fluorescence spectrometer, the agreement is remarkable
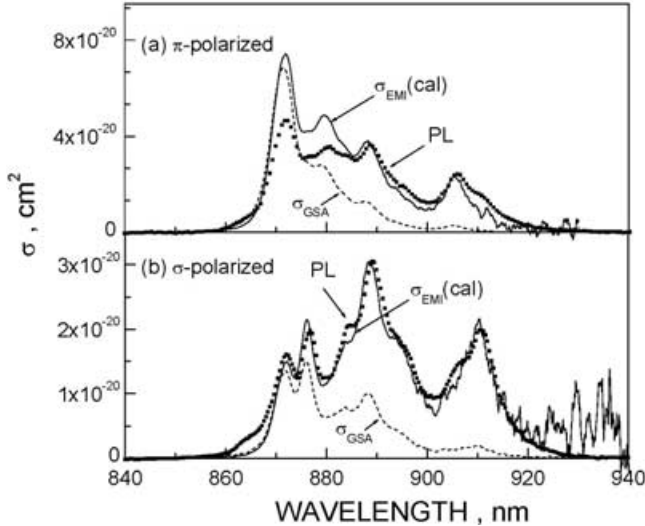

Figure 5. Comparison of the 300 K calculated emission cross-sections, σ_{EMI}(cal) (continuos lines) and the 300 K photoluminescence spectral distribution, PL (dots), of the $^4F_{3/2} \rightarrow {}^4I_{9/2}$ transition of Nd^{3+} in NBW. The $^4F_{3/2}$ ground state absorptions, σ_{GSA} (dashed line), are given for comparison: (a) π-polarized; (b) σ-polarized.

for the σ polarization. The slight deviation at low wavelengths in the π spectra is due to the experimental uncertainty in sample orientation.

The σ_{EMI} values of the $^4F_{3/2} \rightarrow {}^4I_J$ ($J = 11/2, 13/2$) are now calculated by using the photoluminescence intensities, I, given in figure 2 and the Füchtbauer–Ladenburg method [22]

$$\sigma_{EMI} = \sigma_{EMI}^{REF} \frac{I}{I_{REF}} \frac{\lambda^5}{\lambda_{REF}^5}, \qquad (10)$$

where σ_{EMI}^{REF}, I_{REF} and λ_{REF} are reference values taken from the $^4F_{3/2} \rightarrow {}^4I_{9/2}$ emission.

Although not shown for the sake of brevity, π-polarized $^4F_{3/2}$ emissions of Nd in NBW always have larger peak cross-sections than σ-polarized ones. Table 3 summarizes the ground-state absorption and emission cross-sections at a few significant wavelengths.

It is worth noting that the highest emission cross-section achieved for Nd in NBW, namely $\sigma_{EMI}^{\pi}(\lambda = 1060.9 \text{ nm}) = 16 \times 10^{-20} \text{ cm}^2$, is not very far from those reported for Nd-doped YAG ($\sigma_{EMI} = 28 \times 10^{-20} \text{ cm}^2$ [23]) and Nd-doped $KGd(WO_4)_2$ ($\sigma_{EMI} = 35 \times 10^{-20} \text{ cm}^2$ [24]). In fact, it is similar to those of other Nd laser hosts, i.e. NAB ($\sigma_{EMI}^{\sigma-\pi} \approx 16 - 14 \times 10^{-20} \text{ cm}^2$ [25]) and YLF ($\sigma_{EMI}^{\pi} = 18 \times 10^{-20} \text{ cm}^2$ [23]) and larger than those reported in other disordered double tungstates or molybdates, for instance $KLa(MoO_4)_2$ ($\sigma_{EMI}^{\pi} = 9.7 \times 10^{-20} \text{ cm}^2$) [12], $NaY(WO_4)_2$ ($\sigma_{EMI}^{\pi} \approx 6 \times 10^{-20} \text{ cm}^2$) [1]. This result could suggest that the degree of disorder (or number of Nd sites with different crystal field) in NBW is larger than in the ordered $KGd(WO_4)_2$ but lower than in $KLa(MoO_4)_2$ and $NaY(WO_4)_2$ crystals.

The difference between the radiative lifetime calculated by the JO approach and the experimental lifetimes of a level is accounted for the presence of non-radiative processes, namely multiphonon emission and energy transfer, $\tau_{exp}^{-1} = \tau_{rad}^{-1} + \tau_{ph}^{-1} + \tau_C^{-1}$, where τ_{ph}^{-1} is the multiphonon relaxation rate and τ_C^{-1} is the energy transfer rate.

Since the experimental lifetime calculated at low temperature and low Nd concentration basically agrees with the radiative lifetime of the JO calculation, intra-ionic or ion–lattice transfer non-radiative decays of the Nd^{3+} $^4F_{3/2}$ level in NBW are negligible. For low Nd concentration, the temperature dependence of the $^4F_{3/2}$ experimental lifetime shows the activation of some thermally excited non-radiative paths (see figure 3). This is described by a multiphonon relaxation rate given by [26]

$$\tau_{ph}^{-1}(T) = \tau_{ph}^{-1}(0)(1 + n)^{ph}, \qquad (11)$$

where $n = \left[\exp\left(\hbar\omega/k_B T\right) - 1\right]^{-1}$ with $\hbar\omega$ being the energy of the phonon emitted, often taken as the cutting

Table 3. 300 K ground state absorption cross-sections, σ_{GSA}, and emission cross-sections, σ_{EMI}, for a few significant transitions related to the Nd³⁺ laser operation.

$^4I_{9/2} \rightarrow$		$^4G_{9/2} + {}^2K_{13/2} + {}^2G_{7/2}$	$^4G_{5/2} + {}^4G_{7/2}$	$^2H_{9/2} + {}^4F_{5/2}$	$^4F_{3/2}$
λ (nm), σ_{GSA} ($\times 10^{-20}$ cm²)	σ	525.4, 41.0	586.0, 29.0	804.7, 7.0	876.1, 1.3
	π	531.4, 47.5	574.3, 84.0	803.1, 38.0	871.9, 5.3
		526.4, 47.5	584.5, 88.2		

$^4F_{3/2} \rightarrow$		$^4I_{9/2}$	$^4I_{11/2}$	$^4I_{13/2}$
λ (nm), σ_{EMI} ($\times 10^{-20}$ cm²)	σ	888.6, 3.0	1063.9, 9.9	1340.2, 3.3
	π	871.8, 7.0	1060.9, 16.3	1341.1, 4.3

frequency in the Raman or infrared spectra and *ph* is the number (not necessary an integer) of phonons required to maintain the energy conservation in a non-radiative transition between the level separated by ΔE. The energy distance between the $^4F_{3/2}$ and the low-lying $^4I_{15/2}$ levels is $\Delta E = 5075\ cm^{-1}$ [9]. Assuming that the phonon emitted is the largest one of the Raman spectrum of NBW [2], namely $\hbar\omega = 920\ cm^{-1}$, the number of emitted phonons must be $ph = 5$–6. The continuous line of figure 3 shows the fit of the $^4F_{3/2}$ lifetime temperature dependence. The agreement confirms that multiphonon emission is the main non-radiative decay path at this Nd concentration.

At higher Nd concentrations the energy transfer between Nd and other surrounding Nd ions should eventually become an important non-radiative de-excitation path. A comparison of the 300 K experimental lifetimes with increasing Nd concentration, figure 4, shows that for $[Nd] = 3.6 \times 10^{18}\ cm^{-3}$ only a slight lifetime reduction is observed, and the exponential character of the decay is preserved. At higher neodymium concentration, i.e. $[Nd] = 4.0 \times 10^{19}\ cm^{-3}$, some slight departure of the single exponential behaviour seems to appear in figure 4(*c*).

This behaviour can be accounted for by the onset of energy transfer expressed by [27]

$$I(t) = I(t=0)\ \exp\left[\frac{-t}{\tau_0} - \Gamma\left(1 - \frac{3}{s}\right)\frac{[Nd]}{c_0}\left(\frac{t}{\tau_0}\right)^{3/s}\right],$$

(12)

where $I(t)$ is the temporal intensity evolution of the emitted light, τ_0 is the decay time in the absence of energy transfer, $\Gamma(x)$ is the gamma function, s describes the transfer mechanism and $c_0 = 3/4\pi R_C^3$, R_C being the distance for which the energy transfer rate equals the spontaneous decay rate. A good linear $\ln[I(t)/I(0)] + t/\tau_0$ versus $t^{3/s}$ fit was found for $s = 6$ (electric dipole–dipole interaction). Using this value the fit of the experimental decay in figure 4(*c*) with equation (12) gave $R_C = 9.6$ Å. This critical distance is much shorter than the average Nd–Nd distance, ≈ 18 Å, corresponding to the doping level used. This result could be anticipated in view of the still incipient reduction of the lifetime in comparison to the lowest neodymium concentration available. Therefore, the non-radiative energy transfer losses at the highest Nd concentration considered are small and further emission intensity enhancement could be expected for $[Nd] > 4.0 \times 10^{19}\ cm^{-3}$ if the crystal quality was preserved.

6. Conclusions

We have shown that efficient optical absorption and emission can be obtained at room temperature in Nd^{3+} doped $NaBi(WO_4)_2$. The absorption and emission are strongly polarized as expected from the uniaxial and non centrosymmetric character of the host. Despite the coexistence of a range of locally different Nd^{3+} optical centres, responsible for the observed band broadening, the peak emission cross-section obtained, $\sigma^\pi \approx 16 \times 10^{-20}\ cm^2$, is in the range for Nd crystalline laser hosts, $\sigma \approx 15$–$35 \times 10^{-20}\ cm^2$. The high $^4F_{3/2}$ emission quantum efficiency, $\eta = \tau_{exp}/\tau_{rad} \approx 0.85$, achieved at 300 K for $[Nd] = 4.0 \times 10^{19}\ cm^{-3}$, suggests that additional improvements can still be pursued by increasing the Nd concentration in the crystal, although the accomplishment of this goal requires further development of the crystal growth methods.

References

[1] KAMINSKII, A. A., EICHLER, H. J., UEDA, K., KLASSEN, N. V., REDKIN, B. S., LI, L. E., FINDEISEN, J., JAQUE, D., GARCÍA SOLÉ, J., FERNÁNDEZ, J., and BALDA, R., 1999, *Appl. Opt.*, **38**, 4533.

[2] HANUZA, J., BENZAR, A., HAZNAR, A., MACZKA, M., PIETRASZKO, A., and VAN DER MAAS, J. H., 1996, *Vib. Spec.*, **12**, 25.

[3] HANUZA, J., HARNAR, A., MACZKA, M., PIETRASZKO, A., LEMIEC, A., VAN DER MAAS, J. H., and LUTZ, E. T. G., 1997, *J. Raman Spectrosc.*, **28**, 953.

[4] RICO, M., VOLKOV, V., CASCALES, C., and ZALDO, C., 2002, *Chem. Phys.*, **279**, 73.

[5] KAMINSKII, A. A., BAGAYEV, S. N., UEDA, K., NISHIOKA, H., KUBOTA, Y., CHEN, X., and KHOLOV, A., 1995, *Jpn. J. appl. Phys.*, **34**, L1461.

[6] KAMINSKII, A. A., 1996, *Crystalline Lasers: Physical Processes and Operating Schemes* (Boca Raton, New York, London, Tokyo: CRC Press).

[7] VOLKOV, V., and ZALDO, C., 1999, *J. cryst. Growth*, **206**, 60.

[8] VOLKOV, V., RICO, M., MÉNDEZ-BLAS, A., and ZALDO, C., 2002, *J. phys. chem. Solids*, **63**, 95.

[9] MÉNDEZ-BLAS, A., VOLKOV, V., CASCALES, C., and ZALDO, C., 2001, *J. Alloys Compounds*, **323**, 315. In this work figure 1 caption should read $[Nd] = 0.3 \times 10^{19}\ cm^{-3}$ and the $^4F_{3/2}$ π spectrum should be multiplied by a factor of 2.5.

[10] KADONO, K., SHOJIYA, M., TAKAHASHI, M., HIGUCHI, H., and KAWAMOTO, Y., 1999, *J. non-cryst. Solids*, **259**, 39.

[11] TANNER, P. A., QUAGLIANO, J., and RICHARDSON, F. S., 1991, *J. chem. Soc. Faraday Trans.*, **87**, 1707.

[12] CAVALLI, E., ZANNONI, E., MUCCHINO, C., CAROZZO, V., TONCELLI, A., TONELLI, M., and BETTINELLI, M., 1999, *J. opt. Soc. Am. B*, **16**, 1958.

[13] CHENG, Z., ZHANG, S., FU, K., LIU, J., and CHEN, H., 2001, *Jpn. J. appl. Phys.*, **40**, 4038.

[14] JUDD, B. R., 1962, *Phys. Rev.*, **127,** 750.
[15] OFELT, G. S., 1962, *J. chem. Phys.*, **37,** 511.
[16] CARNALL, W. T., GOODMAN, G. L., RAJNAK, K., and RANA, R. S. J., 1989, *Chem. Phys.*, **90,** 3443.
[17] KRUPKE, W. F., 1971, *IEEE J. quantum Electron.*, **QE-7,** 153.
[18] CARNALL, W. T., FIELDS, P. R., and WYBOURNE, B. G., 1965, *J. chem. Phys.*, **42,** 3797.
[19] LOMHEIM, T. S., and DE SHAZER, L. G., 1978, *J. appl. Phys.*, **49,** 5517.
[20] MEHTA, V., AKA, G., DAWAR, A. L., and MANSINGH, A., 1999, *Opt. Mater.*, **12,** 53.
[21] McCUMBER, D. E., 1964, *Phys. Rev.*, **136,** A954.
[22] AULL, B. F., and JENSSEN, H. P., 1982, *IEEE J. quantum Electron.*, **18,** 925.
[23] KOECHNER, W., 1996, *Solid-State Laser Engineering, Springer Series in Optical Science*, Vol. 1 (Berlin: Springer).
[24] MUSSET, O., and BOQUILLON, J. P., 1997, *Appl. Phys. B,* **64,** 503.
[25] JAQUE, D., ENGUITA, O., CALDIÑO, U., RAMÍREZ, M. O., GARCÍA-SOLÉ, J., ZALDO, C., MUÑOZ-SANTIUSTE, J. E., JIANG, A. D., and LUO, Z. D., 2001, *J. appl. Phys.*, **90,** 561.
[26] RISEBERG, L. A., and MOSS, H. W., 1968, *Phys. Rev.*, **174,** 429.
[27] INOKUTI, M., and HIRAYAMA, F., 1965, *J. chem. Phys.*, **43,** 1978.